Atmos. Chem. Phys. Discuss., 15, 21583–21606, 2015
www.atmos-chem-phys-discuss.net/15/21583/2015/
doi:10.5194/acpd-15-21583-2015

Atmospheric Chemistry and Physics Discussions

Measurement-based direct radiative effect by brown carbon over Indo-Gangetic Plain

A. Arola[1], G. L. Schuster[2], M. R. A. Pitkänen[1,3], O. Dubovik[4], H. Kokkola[1], A. V. Lindfors[1], T. Mielonen[1], T. Raatikainen[5], S. Romakkaniemi[1], S. N. Tripathi[6,7], and H. Lihavainen[5]

[1]Finnish Meteorological Institute, Kuopio, Finland
[2]NASA Langley Research Center Hampton, VA, USA
[3]Department of Applied Physics, University of Eastern Finland, Kuopio, Finland
[4]LOA, Université de Lille1/CNRS, Villeneuve d'Ascq, France
[5]Finnish Meteorological Institute, Helsinki, Finland
[6]Department of Civil Engineering, Indian Institute of Technology, Kanpur, India
[7]Centre for Environmental Science and Engineering, Indian Institute of Technology, Kanpur, India

Received: 1 June 2015 – Accepted: 15 July 2015 – Published: 10 August 2015

Correspondence to: A. Arola (antti.arola@fmi.fi)

Published by Copernicus Publications on behalf of the European Geosciences Union.

Abstract

The importance of light absorbing organic aerosols, often called brown carbon (BrC), has become evident in recent years. However, there are relatively few measurement-based estimates for the direct radiative effect of BrC so far. In those earlier studies, the AErosol RObotic NETwork (AERONET) measured Aerosol Absorption Optical Depth (AAOD) and Absorption Angstrom Exponent (AAE) have been exploited. However, these two pieces of information are clearly not sufficient to separate properly carbonaceous aerosols from dust, while imaginary indices of refraction would contain more and better justified information for this purpose. This is first time that the direct radiative effect (DRE) of BrC is estimated by exploiting the AERONET-retrieved imaginary indices. We estimated it for four sites in Indo-Gangetic Plain (IGP), Karachi, Lahore, Kanpur and Gandhi College. We found a distinct seasonality, which was generally similar among all the sites, but with slightly different strengths. The monthly warming effect up to 0.5 $W m^{-2}$ takes place during spring season. On the other hand, BrC results in overall cooling effect in the winter season, which can reach levels close to $-1 W m^{-2}$. We then estimated similarly also DRE of black carbon and total aerosol, in order to assess the relative significance of BrC radiative effect in the radiative effects of other components. Even though BrC impact seems minor in this context, we demonstrated that it is not insignificant and moreover that it is crucial to perform spectrally resolved radiative transfer calculations to obtain good estimates for DRE of BrC.

1 Introduction

Aerosols affect the Earth's climate both directly (by scattering and absorbing radiation) and indirectly (by serving as nuclei for cloud droplets). Currently, aerosol forcing is the largest uncertainty in assessing the anthropogenic climate change (Myhre et al., 2013). Specifically, the role of carbonaceous aerosols is poorly understood. These particles can be divided into two categories: (1) black carbon (BC) is the main absorbing compo-

ACPD
15, 21583–21606, 2015

nent present in atmospheric aerosols, (2) organic carbon (OC) represents a significant and sometimes major (20–90 %) mass fraction of the sub-micron aerosol (Kanakidou et al., 2005; Zhang et al., 2007). Organic carbon has been most often assumed, in global models for instance, to be non or only slightly absorbing component. However, there is a growing evidence that a substantial amount of organic aerosols absorb at UV and visible wavelengths, particularly strongly at shorter wavelengths (e.g., Kirchstetter et al., 2004; Martins et al., 2009). Nevertheless, so far there are only relatively few measurement-based estimates for the direct radiative effect (DRE) of absorbing organic carbon, often called brown carbon, BrC. Both Chung et al. (2012) and Feng et al. (2013) exploited AErosol RObotic NETwork (AERONET) measurements to derive the radiative effect by BrC, the former used an approach to separate dust and carbonaceous aerosols based on AERONET-measured Absorption Angstrom Exponent (AAE), while the latter accounted for short-wave enhanced absorption by BrC in their global model and demonstrated an improved correspondence of modeled Aerosol Absorption Optical Depth (AAOD) and AERONET measurements, when BrC absorption was included in the model.

The approach of Chung et al. (2012) has evident difficulties in separating dust and carbonaceous by using AAE, and arguably an approach using AERONET-retrieved imaginary indices of refraction would be more justified, as discussed also in Schuster et al. (2015a, b). We estimated the BrC fractions by using the method of Schuster et al. (2015a) for four AERONET sites in Indo-Gangetic Plain (IGP), Karachi, Lahore, Kanpur and Gandhi College, and then calculated the corresponding radiative effect by BrC. We moreover calculated similarly the DRE of BC and total aerosol, in order to assess the relative significance of BrC radiative effect in carbonaceous or total aerosol radiative effects.

ACPD
15, 21583–21606, 2015

2 Data and Methods

2.1 AERONET data

AERONET (AErosol RObotic NETwork) is a globally distributed network of automatic sun and sky scanning radiometers that measure at several wavelengths, typically centered at 0.34, 0.38, 0.44, 0.50, 0.67, 0.87, 0.94, and 1.02 µm. Each band has a full width of approximately 0.010 µm at half maximum (FWHM). All of these spectral bands are utilized in the direct Sun measurements, while four of them are used for the sky radiance measurements, 0.44, 0.67, 0.87 and 1.02 µm. Spectral aerosol optical depth (AOD) is obtained from direct sun measurements, and inversion products of other aerosol optical properties, such as single scattering albedo (SSA), refractive indices and the column integrated aerosol size distributions above the measurement site are provided at the sky radiance wavelengths (Holben et al., 1998).

The estimated uncertainty in AOD (Level 2) is 0.01–0.02 and is primarily due to the calibration uncertainty (Eck et al., 1999). The uncertainty in complex index of refraction depends on AOD, Dubovik et al. (2000) estimated errors on the order of 30–50 % for the imaginary part and 0.04 for the real part of the refractive index for the cases of high aerosol loading (AOD larger than 0.5). Aerosol loading is very high in IGP region, therefore these uncertainty estimates are likely representative for our AERONET sites as well.

Since the shortest sky radiance wavelength is 440 nm, AERONET wavelengths are not ideal to detect BrC absorption, which is much stronger at shorter than 440 nm wavelengths. However, it is also stressed that AOD is very high for all sites that were analyzed, allowing for sufficient robustness in the retrieved spectral signal in the imaginary refractive index.

In our study, we used Level 1.5 data of size distributions and refractive indices at four retrieval wavelengths 0.44, 0.67, 0.87 and 1.02 µm to estimate the radiative effect by BrC. However, when we selected the data from the Level 1.5 inversion product, we applied all the other level 2.0 AERONET criteria except for the AOD threshold. In

ACPD
15, 21583–21606, 2015

other words, we applied otherwise the same rigorous quality control that is required for Level 2 data, but we only relaxed the AOD requirement at 440 nm from 0.4 to 0.2. We selected on purpose also these cases of possibly somewhat lower AOD, in order to not bias our sample, and thus estimate of DRE, towards higher aerosol loading. However, AOD at 440 nm is typically above 0.4 in IGP region, so the set of refractive indices that we included turned out to be insignificantly different to that of the "full" Level 2 (not shown). Moreover, that AOD threshold requirement is not applied in Level 2 size distributions, which means that we included only Level 2 size distributions.

We included four AERONET sites for our data analysis, covering wide conditions in the Indo-Gangetic Plain (IGP): Karachi and Lahore in Pakistan, and Kanpur and Gandhi College in India. The measurements covered the following time periods, Gandhi College: April 2006–March 2010, Kanpur: January 2001–April 2012, Karachi: September 2006–August 2011, Lahore: April 2007–October 2011. Figure 1 shows the locations of these sites overlaid in the annual mean AOD map from MODIS Terra. In the IGP there are large local emissions of aerosols from various sources: heavy particulate pollution from industrial sources, strong vehicular emissions, use of fossil fuels, and widespread biomass and agricultural crop residue burning. In addition, the IGP is strongly affected by seasonal (pre-monsoon) mineral dust transported mainly from the Thar desert (e.g., Jethva et al., 2005; Ram et al., 2010; Kedia et al., 2014). The seasonal monsoon rains are extremely vital for IGP and strongly anchors one commonly used way to divide the year into four distinct seasons: winter (December–February), premonsoon (March–May), monsoon (June–August), and postmonsoon (September–November). The strong and seasonally varying aerosol sources in IGP result in a very distinct geographical pattern of elevated AOD, bounded in north by Himalayan foothills.

Figure 2 shows the monthly mean AOD and SSA at 440 nm for our study sites. It is noted that this data set includes all AOD values without the AOD threshold of 0.2 that we applied for refractive indices and also for SSA shown in the lower plot. This figure then further illustrates that the AOD levels are typically high and why our selected set of refractive indices became very close to that of "full" Level 2.

ACPD
15, 21583–21606, 2015

2.2 Retrieval of BrC from AERONET measurements

Schuster et al. (2005) developed an approach to retrieve black carbon concentration and specific absorption from AERONET retrievals of imaginary refractive indices and it was further extended by Arola et al. (2011) to include also BrC. Recently, this method has been further extended by Schuster et al. (2015a) to simultaneously include carbonaceous aerosols (both BC and BrC) and also mineral dust in both fine and coarse modes separately.

Since the main details of the methodology are comprehensively described elsewhere, particularly in Schuster et al. (2015a), only main points are summarized below. The approach is based on the best match between modeled imaginary index and those retrieved by AERONET at four inversion wavelengths. For the modeled case, a scattering host is assumed to contain the following absorbing components: black carbon, brown carbon, hematite, and goethite. It is emphasized that this approach is able to detect only a subset of total organic carbon that is present, the part of absorbing organic carbon (BrC). Therefore, the BrC/BC ratios that we can infer from AERONET are not directly comparable with OC/BC ratios available from in-situ measurements. Table 1 provides the assumed refractive indices for each of these components. It is noted that while the most recent version of Schuster et al. (2015a) uses Maxwell–Garnett as the mixing rule for refractive indices, volume averaging was assumed in the data set used in our analysis. Arguably, given the scope of our study, the choice of the mixing rule is not very essential, as long as applied consistently both in the AERONET retrieval and in our radiative transfer calculations. Moreover, it has been shown that the volume averaging results in very reasonable performance in many cases, as demonstrated for instance in Lesins et al. (2002).

The AERONET-retrieved imaginary refractive indices at four wavelengths form the basis to retrieve the fractions of absorbing components, including BrC. The retrieval initially populates the fine mode with BC and BrC and the coarse mode with dust components (hematite and goethite). However, in some cases in order to reach a realistic fit

ACPD
15, 21583–21606, 2015

with the AERONET-retrieved imaginary indices, some of the fine mode has to additionally include iron oxides (hematite and goethite) and likewise some of the coarse mode can include carbonaceous aerosols. The average imaginary index of the three longest wavelengths (670, 870, 1020 nm), at red and near-infrared and hereinafter referred to by k_{RNIR}, determines the black carbon fraction of the fine mode, for instance, while the difference between the imaginary index at 440 nm and k_{RNIR} is due to the presence of BrC. Figure 3 shows the monthly mean values of imaginary index at 440 nm and the difference between $k_{440\,nm}$ and k_{RNIR}, in the a and b panels, respectively. Table 2 gives the number of imaginary indices that was included for each site to form the monthly means. Since we use spectral imaginary index to derive BC and BrC volume fractions, there is understandably a visible similarity between BC fractions and k_{RNIR} (between panels a and c) and also BrC fractions and the difference between imaginary index at 440 nm and RNIR (between panels b and d). The lowest panels, in turn, show the columnar concentrations of BC and BrC. These were obtained by multiplying the BC and BrC volume fractions by AERONET-measured total volume and by the assumed densities. The densities of 1.8 and 1.2 g cm^{-3} were assumed for BC and BrC, respectively.

There is a significant seasonality in both components of carbonaceous aerosols, particularly in BC, largest fractions occurring in the winter and late fall seasons. This BC seasonality agrees well with the seasonal pattern that has been obtained by the surface measurements in IGP (Ram et al., 2010), who observed a very distinct BC seasonality. Moreover, they observed similar seasonal patterns for both BC and OC, highest concentrations in late fall/winter due to various sources of carbonaceous aerosols, biomass burning and wood fuel burning for domestic use, for instance. As noted before, we can only detect absorbing OC via AERONET, so our BrC pattern cannot be, therefore, directly compared with these available OC measurements. However, generally our BrC seasonality agrees also rather well with seasonality of OC in IGP observed by (Ram et al., 2010), while the clearest difference seems to be in spring, when AERONET-based BrC levels are enhanced. As shown by Vadrevu and Lasko (2015), for instance,

ACPD
15, 21583–21606, 2015

in IGP there is a bi-modal burning season, peaking in the spring and late fall/winter, this is captured by our BrC retrievals, suggesting that a large fraction of OC emissions in spring and late fall include brown carbon.

2.3 Calculation of the radiative effect

The radiative transfer calculations were performed by using the libRadtran package (Mayer and Kylling, 2005). We used two-stream solver and correlated-*k* approximation of Kato et al. (1999) with bands from 1 to 31 (from 240.1 to 3991 nm), to cover the entire short-wave (SW) range. The direct radiative effect of BrC, DRE of BrC, at the top of the atmosphere (TOA) was calculated on a monthly basis, as the difference between two cases: including all aerosols and excluding BrC. The former was based on monthly mean size distribution and refractive index, while the latter set was formed by excluding the volume fraction of BrC. By excluding the BrC fraction, both refractive index and size distribution were then modified. The refractive index for "non-BrC" case was created by volume averaging mixing rule and including all the other components except for BrC (the scattering host, black carbon, goethite and hematite). The volume size distribution of "non-BrC" case was formed by reducing the volume in all size ranges by the volume fraction of BrC, separately in the fine and coarse modes. By defining DRE of BrC in this fashion, aerosols are considered internally mixed, which is also the case in AERONET inversion methods. We adopted similar approach to calculate additionally DRE of BC and total aerosol.

Size distributions and refractive indices were then used for calculating the aerosol optical properties for the non-BrC mixture, which was done by utilizing the spheroid aerosol model by Dubovik et al. (2002). The model is consistent with the one used for the retrieval of AERONET products, assuming a portion of the aerosols being spheroids, as described by Dubovik et al. (2006). This way both the "all aerosols" mixture and the "non-BrC" mixture were described by their respective spectral AOD, SSA and asymmetry parameter, which were finally used estimating the DRE of BrC. For the calculations of aerosol direct radiative effect, surface albedo is also a very crucial input.

ACPD
15, 21583–21606, 2015

In our simulations we used monthly spectral solar zenith angle dependent albedo from AERONET inversion product (thus MODIS-based albedo). The DRE of BrC (and BC and total aerosol) at TOA was simulated with one hour time step over a 24 h diurnal cycle with solar insolation of the 15th day of each month.

3 Results

Figure 4 shows our simulated radiative effects by BrC in the lowest panel, while the upper and middle panels include relevant parameters to interpret these results. The difference in AOD at 440 nm (in blue) and at RNIR (average of 670–1020, in red) between the simulations with and without BrC is shown in the upper panel. Middle panel shows similar results for SSA, which are particularly relevant quantities now to understand whether the overall effect is warming or cooling, when BrC is added in. It is emphasized that while brown carbon is absorbing at the shortest wavelengths, determined by the measurement at 440 nm in our case, it is almost purely scattering at RNIR wavelengths. Therefore, when BrC is included, there are typically two spectrally competing effects taking place, warming at the shortest and cooling at the longer wavelengths. And we can detect these effects also in the middle panel of the Fig. 4. In principle, the scattering coefficient at RNIR increases when BrC is added, while the absorption coefficient remains close to a constant. Therefore, SSA (= scattering / [scattering + absorption]) also increases and the SSA difference at RNIR, shown by the dashed red lines, is therefore essentially always positive. On the other hand, both scattering and absorption coefficients increase upon addition of BrC at the 440 wavelength. Hence, SSA decreases with addition of BrC at that wavelength, since scattering and absorption combined increases more than scattering alone. Thus, the blue lines are always negative.

The relative strength of these spectrally separated cooling and warming effects will eventually determine whether the overall spectrally integrated shortwave direct effect is cooling or warming. And the strength of these both effects, in turn, depends on the

ACPD
15, 21583–21606, 2015

relative fractions of other components present. In our version of absorbing components by Schuster et al. (2015a), volume averaging has been applied, consistently both in the retrieval and when we have formed new refractive indices for "non-BrC" case in our simulations. Therefore, it is also now rather straight-forward to give a quantitative estimate about the changes in the imaginary index with and without BrC at 440 nm and RNIR range for any given fractions of these components. It is now possible to separate BrC influence this way, since we have assumed that BC has a constant refractive index at all wavelengths, where BrC is essentially non-absorbing but absorbs at 440 nm. As can be seen from the Table 1, BC has the largest imaginary index at RNIR wavelengths and therefore the most sensitive change towards cooling at RNIR takes place when BrC is added to the mixture of relatively large amount of black carbon. Figure 5 shows the change in imaginary index (based on volume averaging), both at 440 nm and RNIR range, if BrC is added in. The scale of both BC and BrC volume fractions in this figure was determined by the range retrieved for our IGP sites (in the middle panel of the Fig. 3). It is evident that including BrC results in increase of imaginary index difference at 440 nm, which is a strong function of BrC volume fraction but depends only slightly on the BC fraction. At RNIR range the behavior is quite different, at low enough BC fractions, BrC can result in increase in the imaginary index, however most often the opposite is true. Moreover, this decrease in the imaginary index with increasing BrC volume fraction depends also relatively strongly on the BC volume fraction. This means that for a given BrC fraction, the larger the volume fraction of BC the stronger the cooling effect at RNIR wavelengths.

Our estimated values for DRE of BrC shown in the Fig. 4, and the corresponding changes in SSA (in the middle panels), are best further understood with the help of Fig. 5 and there by the behavior at RNIR in particular. Therefore, the lower panel of Fig. 5 includes additionally the retrieved monthly averaged volume fractions of BC and BrC for each site by lines. The name of the site is indicated next to the month of January, and one is then able to follow the line to focus separately on each month. As can be seen in the middle panel of the Fig. 4, the largest positive SSA differences at RNIR,

ACPD
15, 21583–21606, 2015

when BrC is included, are in Gandhi College in November and Lahore in December. These are also the two cases that are closest to the upper right corner of the Fig. 5b and thus of largest decrease in imaginary index by added BrC, and are therefore also the cases of strongest overall cooling by BrC (most negative cases in the lowest panel of Fig. 4). The spectral SSA changes due to the BrC, that are illustrated in the middle panel of the Fig. 4, mainly determine whether overall cooling or warming takes place. However, the actual magnitude of these spectral cooling and warming contributions, in turn, are also substantially influenced by the absolute BrC fractions in AOD, which are shown in the upper panel of the Fig. 4. It is evident that the large values of BrC optical depths at the end of year in Gandhi College, in addition to the large increase of SSA at RNIR wavelengths, also strongly contribute to the considerable DRE of BrC. Brown Carbon causes cooling in the other sites as well during this time of the year, when BC fractions are at the highest. On the other hand, the warming takes place typically in the spring season in all the sites, when BC fractions are lower, but BrC fractions are at relatively high levels (shown in the Figs. 3 and 5). To summarize, the common pattern is the warming by BrC at spring season and cooling in the late fall and winter (except for Karachi where cooling takes place only in November–December) and this change of sign in the radiative effect by BrC is due to the different relative fractions of BC during spring and late fall seasons.

The annually averaged DRE of BrC is slightly positive for Karachi, while Lahore and Kanpur has slight cooling by BrC. The annually averaged negative forcing in Gandhi College is somewhat more profound due to the strongest cooling in November–December period. The strongest cooling is due to the highest total BrC concentrations and thus AOD corresponding to the BrC during this period, as can be seen from the upper panel of the Fig. 4.

As discussed above, whether the spectrally integrated SW direct radiative effect by BrC results in cooling or warming is determined by the relative strength of two opposing effects, warming at shorter wavelengths and cooling at RNIR range. Thus it is crucial to properly take both of these spectral effects into account, which is often true for total

ACPD
15, 21583–21606, 2015

aerosol DRE calculations as well. However, it has been also common to estimate the optical properties at mid-visible only and then apply some simple approximations and assumptions to account for spectral dependence in direct radiative effect calculations (e.g., Chylek and Wong, 1995; Haywood and Shine, 1995). Therefore, we wanted to also assess how well DRE based on mid-visible range only could represent the entire SW range. We repeated our calculations for DRE of BrC, but using Kato band #10 only, since it has the central wavelength at 544.8 nm (range from 540 to 549.5 nm). We estimated additionally direct radiative effect of BC and total aerosol, using identical approach that we described above for BrC. Thus DRE of BC, for instance, was based on two radiative transfer runs: case of all aerosols and without BC. We then calculated the mean ratio of DRE from the following two runs (separately for BrC, BC and total aerosol cases): (1) actual spectrally resolved radiative transfer calculation including all the Kato bands, i.e. by the same approach we have applied in our results shown earlier, (2) radiative effect from a single Kato band #10 only. This mean ratio was then used as a conversion factor to get a full SW DRE from a single-band DRE radiative transfer runs, and to make these two approaches comparable. Figure 6 shows the DRE in Kanpur from these two cases: (1) actual spectrally resolved radiative transfer calculation including all the Kato bands, (2) radiative effect from a single Kato band #10 only, but scaled to represent full SW.

It is evident that a single wavelength approach can produce a rather stable estimate for BC radiative effect, the relative error is within ±10 %, which is understandable given spectrally invariant imaginary index of BC. On the other hand, both BrC and total aerosol cases can reach significantly higher relative differences. SW radiative effects of BrC and total aerosol include typically wavelength ranges of both cooling and warming effects that a single wavelength approach cannot therefore properly capture. Spectral dependence of DRE of BrC was illuminated above, while the spectral dependence of total aerosol DRE is typically different, for instance in Kanpur SSA is low enough and surface albedo high enough at RNIR range during summer months to produce warming at these longer wavelengths (not shown), although the overall spectrally integrated

ACPD
15, 21583–21606, 2015

total aerosol direct radiative effect is always negative, as shown in the lower panel of the Fig. 6

4 Conclusions

The importance of light absorbing organic aerosols has become evident in recent years. However, there are relatively few measurement-based estimates for the direct radiative effect of BrC so far. In those earlier studies, the AERONET-measured AAOD and AAE have been exploited, while this is the first time that DRE of BrC is estimated by exploiting the AERONET-retrieved imaginary indices. We estimated the radiative effect of BrC for four AERONET sites in Indo-Gangetic Plain (IGP), Karachi, Lahore, Kanpur and Gandhi College. We found a distinct seasonality, which was generally similar among all the sites, but with slightly different strengths. The warming by BrC takes place during spring season, due to the relatively low BC fractions so that the scattering effect by BrC at RNIR does not become significant enough and the absorption at the shortest wavelengths is dominating in the spectrally integrated radiative effect. Opposite is true in late fall and in the winter period, when the BC fractions are more substantial and therefore the cooling effect at RNIR wavelengths becomes more significant in the overall shortwave radiative effect by BrC.

We estimated the DRE of BrC as a difference of two radiative transfer runs: case of all aerosols and without BrC. We estimated the DRE of BC and total aerosol similarly and in that context, it was evident that the role of BrC is relatively minor. Nevertheless, it is not insignificant and also exhibits a distinct seasonality in the four sites we included in our analysis. Therefore, this study stresses the need to account for absorbing OC, not to assume it purely scattering. And it is then particularly crucial to properly account for both warming at the lowest and cooling effect at the longer wavelengths, when forming the overall SW direct radiative effect of BrC.

Acknowledgements. This study was supported by the Academy of Finland (project number 264242).

ACPD
15, 21583–21606, 2015

References

Arola, A., Schuster, G., Myhre, G., Kazadzis, S., Dey, S., and Tripathi, S. N.: Inferring absorbing organic carbon content from AERONET data, Atmos. Chem. Phys., 11, 215–225, doi:10.5194/acp-11-215-2011, 2011. 21588

Chung, C., Ramanathan, V., and Decremer, D.: Observationally constrained estimates of carbonaceous aerosol radiative forcing, P. Natl. Acad. Sci. USA, 109, 11624–11629, 2012. 21585

Chylek, P. and Wong, J.: Effect of absorbing aerosols on global radiation budget, Geophys. Res. Lett., 22, 929–931, 1995. 21594

Dubovik, O., Smirnov, A., Holben, B. N., King, M. D., Kaufman, Y. J., Eck, T. F., and Slutsker, I.: Accuracy assessment of aerosol optical properties retrieval from AERONET sun and sky radiance measurements, J. Geophys. Res., 105, 9791–9806, 2000. 21586

Dubovik, O., Holben, B. N., Lapyonok, T., Sinyuk, A., Mishchenko, M. I., Yang, P., and Slutsker, I.: Non-spherical aerosol retrieval method employing light scattering by spheroids, Geophys. Res. Lett., 29, 54-1–54-4, doi:10.1029/2001GL014506, 2002. 21590

Dubovik, O., Sinyuk, A., Lapyonok, T., Holben, B. N., Mishchenko, M., Yang, P., Eck, T. F., Volten, H., Muñoz, O., Veihelmann, B., van der Zande, W. J., Leon, J.-F., Sorokin, M., and Slutsker, I.: Application of spheroid models to account for aerosol particle nonsphericity in remote sensing of desert dust, J. Geophys. Res.-Atmos., 111, D11208, doi:10.1029/2005JD006619, 2006. 21590

Eck, T., Holben, B., Reid, J. S., Dubovik, O., Smirnov, A., O'Neill, N. T., Slutsker, I., and Kinne, S.: Wavelength dependence of the optical depth of biomass burning urban and desert dust aerosols, J. Geophys. Res., 104, 31333–31349, doi:10.1029/1999JD900923, 1999. 21586

Feng, Y., Ramanathan, V., and Kotamarthi, V. R.: Brown carbon: a significant atmospheric absorber of solar radiation?, Atmos. Chem. Phys., 13, 8607–8621, doi:10.5194/acp-13-8607-2013, 2013. 21585

Haywood, J. M. and Shine, K. P.: The effect of anthropogenic sulfate and soot aerosol on the clear sky planetary radiation budget, Geophys. Res. Lett., 22, 602–606, 1995. 21594

Holben, B. N., Eck, T. F., Slutsker, I., Tanre, D., Buis, J. P., Setzer, A., Vermote, E., Reagan, J. A., Kaufman, Y., Nakajima, T., Lavenu, F., Jankowiak, I., and Smirnov, A.: AERONET – a feder-

ACPD
15, 21583–21606, 2015

ated instrument network and data archive for aerosol characterization, Remote Sens. Environ., 66, 1–16, 1998. 21586
Jethva, H., Satheesh, S. K., and Srinivasan, J.: Seasonal variability of aerosols over the Indo-Gangetic basin, J. Geophys. Res., 110, D21204, doi:10.1029/2005JD005938, 2005. 21587
Kanakidou, M., Seinfeld, J. H., Pandis, S. N., Barnes, I., Dentener, F. J., Facchini, M. C., Van Dingenen, R., Ervens, B., Nenes, A., Nielsen, C. J., Swietlicki, E., Putaud, J. P., Balkanski, Y., Fuzzi, S., Horth, J., Moortgat, G. K., Winterhalter, R., Myhre, C. E. L., Tsigaridis, K., Vignati, E., Stephanou, E. G., and Wilson, J.: Organic aerosol and global climate modelling: a review, Atmos. Chem. Phys., 5, 1053–1123, doi:10.5194/acp-5-1053-2005, 2005. 21585
Kato, S., Ackerman, T., Mather, J., and Clothiaux, E.: The k-distribution method and correlated-k approximation for short-wave radiative transfer model, J. Quant. Spectrosc. Ra., 62, 109–121, 1999. 21590
Kedia, S., Ramachandran, S., Holben, B. N., and Tripathi, S. N.: Quantification of aerosol type, and sources of aerosols over the Indo-Gangetic Plain, Atmos. Environ., 98, 607–619, doi:10.1016/j.atmosenv.2014.09.022, 2014. 21587
Kirchstetter, T. W., Novakov, T., and Hobbs, P. V.: Evidence that the spectral dependence of light absorption by aerosols is affected by organic carbon, J. Geophys. Res., 109, D21208, doi:10.1029/2004JD004999, 2004. 21585
Lesins, G., Chylek, P., and Lohmann, U.: A study of internal and external mixing scenarios and its effect on aerosol optical properties and direct radiative forcing, J. Geophys. Res., 107, AAC5-1–AAC5-12, doi:10.1029/2001JD000973, 2002. 21588
Lu, Z., Streets, D. G., Winijkul, E., Yan, F., Chen, Y., Bond, T. C., Feng, Y., Dubey, M. K., Liu, S., Pinto, J. P., and Carmichael, G. R.: Light absorption properties and radiative effects of primary organic aerosol emissions, Environ. Sci. Technol., 49, 4868–4877, doi:10.1021/acs.est.5b00211, 2015.
Martins, J. V., Artaxo, P., Kaufman, Y. J., Castanho, A. D., and Remer, L. A.: Spectral absorption properties of aerosol particles from 350–2500 nm, Geophys. Res. Lett., 36, L13810, doi:10.1029/2009GL037435, 2009. 21585
Mayer, B. and Kylling, A.: Technical note: The libRadtran software package for radiative transfer calculations – description and examples of use, Atmos. Chem. Phys., 5, 1855–1877, doi:10.5194/acp-5-1855-2005, 2005. 21590
Myhre, G., Shindell, D., Bréon, F.-M., Collins, W., Fuglestvedt, J., Huang, J., Koch, D., Lamarque, J.-F., Lee, D., Mendoza, B., Nakajima, T., Robock, A., Stephens, G., Takemura, H., and

ACPD
15, 21583–21606, 2015

Zhang, T.: Anthropogenic and natural radiative forcing, in: Climate Change 2013: The Physical Science Basis, Contribution of Working Group I to the Fifth Assessment Report of the Intergovernmental Panel on Climate Change, edited by: Stocker, T. F., Qin, D., Plattner, G.-K., Tignor, M., Allen, S. K., Boschung, J., Nauels, A., Xia, Y., Bex, V., and Midgley, P. M., Cambridge University Press, Cambridge, UK and New York, NY, USA, 659–740, 2013. 21584

Ram, K., Sarin, M. M., and Tripathi, S. N., A 1 year record of carbonaceous aerosols from an urban site in the Indo-Gangetic Plain: characterization, sources, and temporal variability, J. Geophys. Res., 115, D24313, doi:10.1029/2010JD014188, 2010. 21587, 21589

Schuster, G. L., Dubovik, O., Holben, B. N., and Clothiaux, E. E.: Inferring black carbon content and specific absorption from Aerosol Robotic Network (AERONET) aerosol retrievals, J. Geophys. Res., 110, D10S17, doi:10.1029/2004JD004548, 2005. 21588

Schuster, G. L., Dubovik, O., and Arola, A.: Remote sensing of soot carbon – Part 1: Distinguishing different absorbing aerosol species, Atmos. Chem. Phys. Discuss., 15, 13607–13656, doi:10.5194/acpd-15-13607-2015, 2015a. 21585, 21588, 21592, 21599

Schuster, G. L., Dubovik, O., Arola, A., Eck, T. F., and Holben, B. N.: Remote sensing of soot carbon – Part 2: Understanding the absorption Angstrom exponent, Atmos. Chem. Phys. Discuss., 15, 20911–20956, doi:10.5194/acpd-15-20911-2015, 2015b. 21585

Vadrevu, K. and Lasko, K.: Fire regimes and potential bioenergy loss from agricultural lands in the Indo-Gangetic Plains, J. Environ. Manage., 148, 10–20, doi:10.1016/j.jenvman.2013.12.026, 2015. 21589

Zhang, Q., Jimenez, J. L., Canagaratna, M. R., Allan, J. D., Coe, H., Ulbrich, I., Alfarra, M. R., Takami, A., Middlebrook, A. M., Sun, Y. L., Dzepina, K., Dunlea, E., Docherty, K., DeCarlo, P. F., Salcedo, D., Onasch, T., Jayne, J. T., Miyoshi, T., Shimono, A., Hatakeyama, S., Takegawa, N., Kondo, Y., Schneider, J., Drewnick, F., Borrmann, S., Weimer, S., Demerjian, K., Williams, P., Bower, K., Bahreini, R., Cottrell, L., Griffin, R. J., Rautiainen, J., Sun, J. Y., Zhang, Y. M., and Worsnop, D. R. : Ubiquity and dominance of oxygenated species in organic aerosols in anthropogenically-influenced Northern Hemisphere midlatitudes, Geophys. Res. Lett., 34, L13801, doi:10.1029/2007GL029979, 2007. 21585

ACPD
15, 21583–21606, 2015

Table 1. Imaginary indices at 440 nm and NIR (average of 670, 870, and 1020 nm) assumed for each component in the retrieval of Schuster et al. (2015a).

Wavelength	BrC	BC	Goethite	Hematite
440	0.063	0.79	0.068	1.23
NIR	0.003	0.79	0.1203	0.127

ACPD
15, 21583–21606, 2015

Table 2. Number of AERONET observations for each month for the four sites. Data was collected for Karachi from September 2006 to August 2011, for Lahore from April 2007 to October 2011, for Kanpur from January 2001 to April 2012 and for Gandhi College from April 2006 to March 2010. Monthly data in parenthesis was not included in the study due to low number of observations.

Month	Karachi	Lahore	Kanpur	Gandhi College
1	121	19	389	(7)
2	105	13	543	23
3	176	107	746	149
4	165	186	535	211
5	136	172	626	307
6	90	139	365	109
7	46	83	49	(8)
8	14	45	62	(5)
9	129	96	253	42
10	239	116	508	72
11	173	114	433	54
12	118	10	466	68

ACPD
15, 21583–21606, 2015

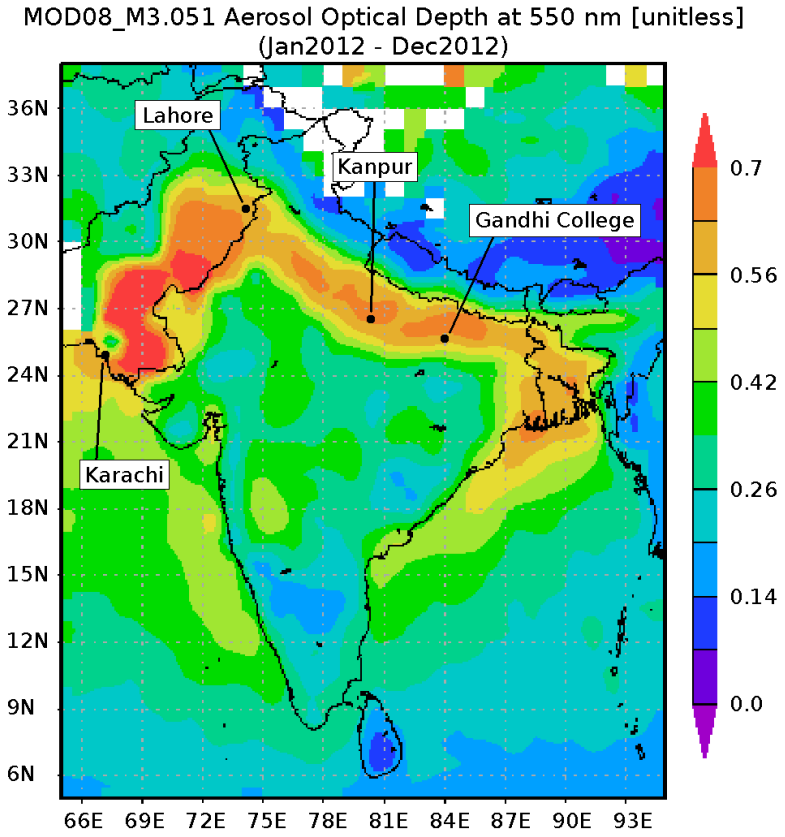

Figure 1. Annual mean AOD from MODIS Terra, with our AERONET study sites overlaid in the map. Source for MODIS data: http://disc.sci.gsfc.nasa.gov/giovanni.

ACPD
15, 21583–21606, 2015

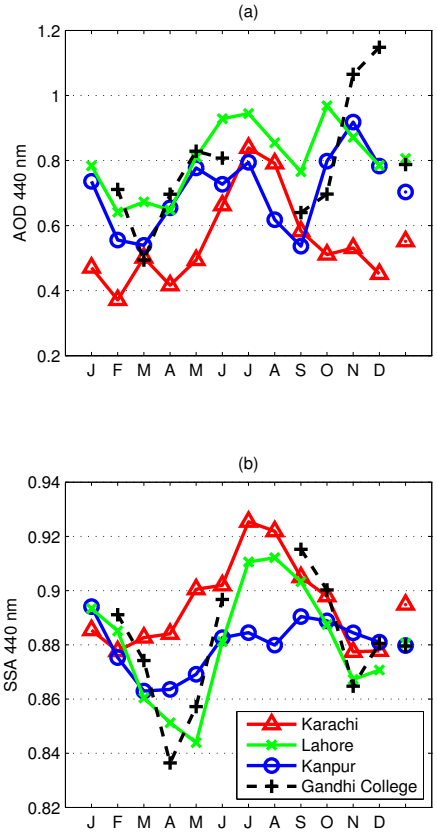

Figure 2. Monthly mean AOD and SSA at 440 nm for our selected AERONET sites. Annual means are indicated by a symbol after December.

ACPD
15, 21583–21606, 2015

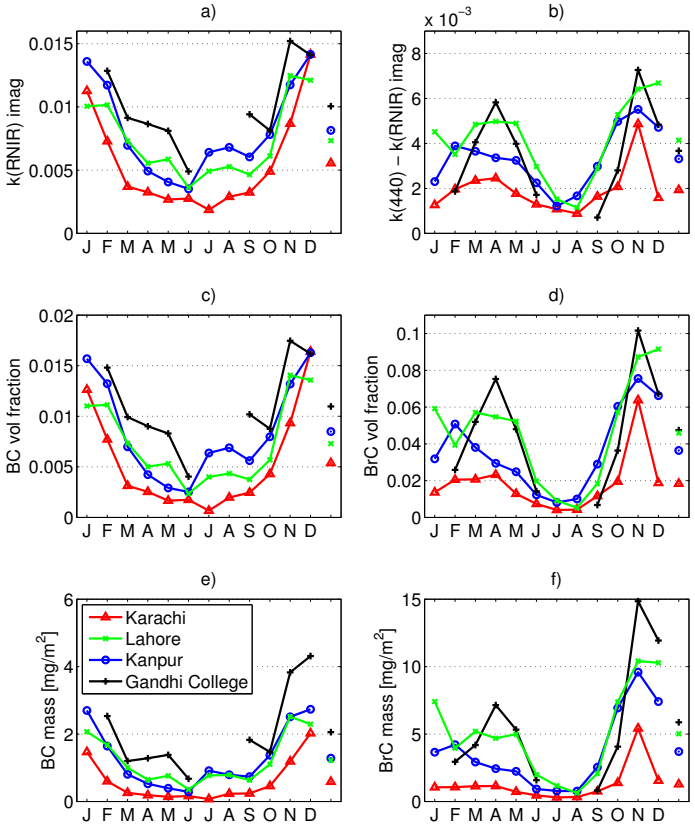

Figure 3. Monthly averages of imaginary indices and the retrieved fraction of carbonaceous aerosols: **(a)** average of imaginary index at 670, 870, and 1020 nm (k_{RNIR}), **(b)** difference between the imaginary index at 440 nm and k_{RNIR}, retrieved volume fractions of **(c)** BC and **(d)** BrC, retrieved columnar concentrations in [mg m^{-2}] of **(e)** BC and **(f)** BrC. Corresponding annual averages are given after December.

ACPD
15, 21583–21606, 2015

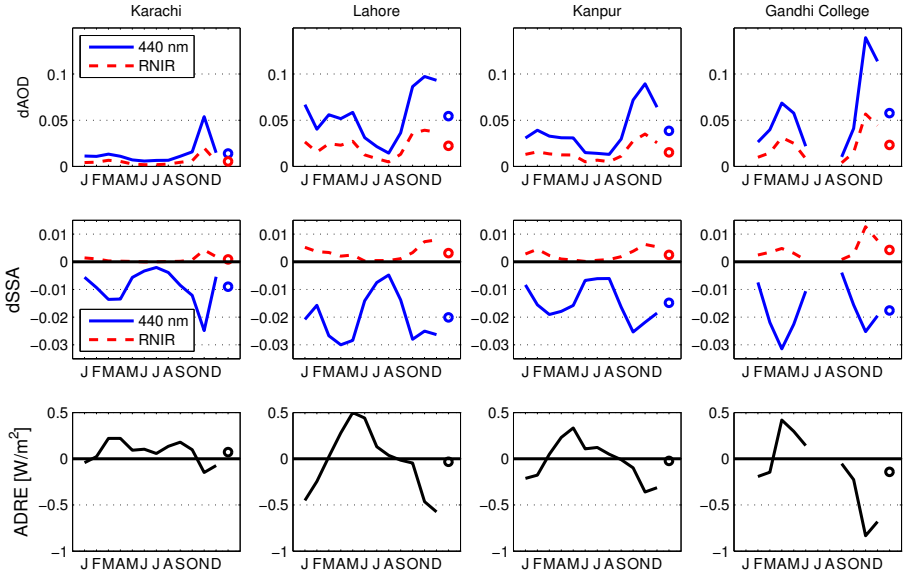

Figure 4. Upper panel: monthly averages of difference in AOD at 440 nm (blue) and at RNIR (red) between simulations with and without BrC. Middle panel: corresponding cases for SSA. Lower panel: monthly average DRE of BrC. Corresponding annual averages are given by the symbol after December.

ACPD
15, 21583–21606, 2015

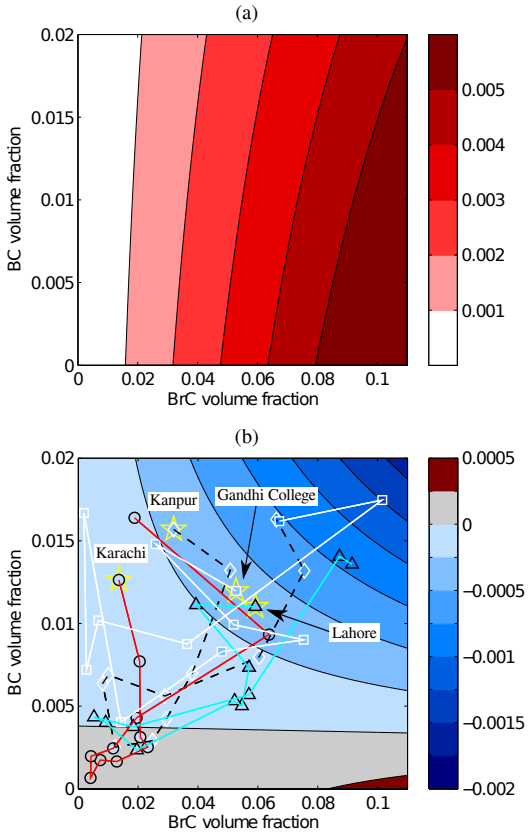

Figure 5. Difference between imaginary index with and without BrC included at 440 nm (upper figure) and at RNIR wavelengths (lower figure) as a function of BC and BrC volume fractions. Monthly mean values of BC and BrC volume fractions are shown for each site by symbols and lines, first month (January) indicated by the yellow star.

ACPD
15, 21583–21606, 2015

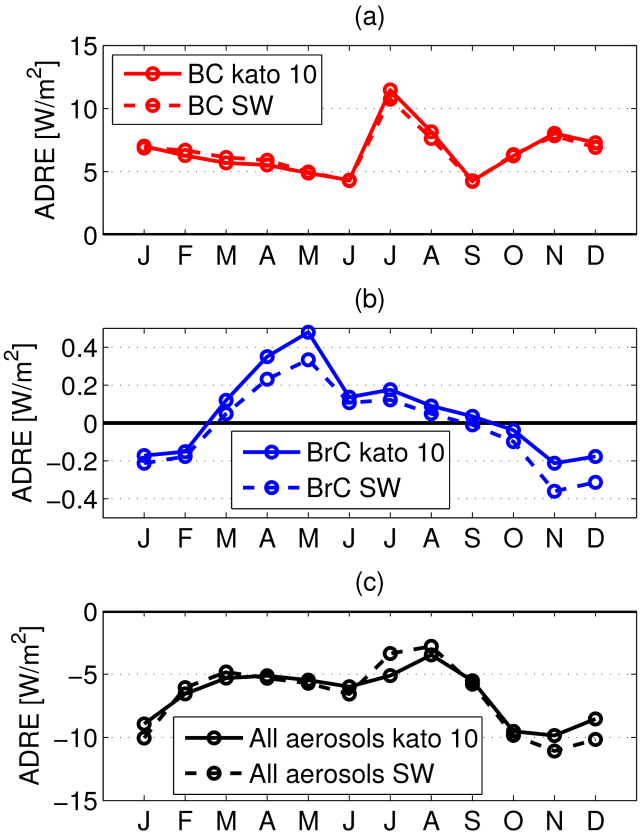

Figure 6. Direct radiative effect in Kanpur based on two spectral ranges of Kato bands: (1) all Kato bands and (2) Kato band #10 (center wavelength at 544.8 nm), but scaled to account for full SW range. Upper panel: for BC, middle panel: for BrC, lower panel: for total aerosol.

ACPD
15, 21583–21606, 2015